

HiSST: 4th International Conference on High-Speed Vehicle Science & Technology



22-26 September 2025, Tours, France

On Shock Layer Instabilities

Vassilis Theofilis1

Abstract

While accurate description of the internal structure of strong shock layers is beyond the scope of the Navier-Stokes equations [9, 15, 4, 2], continuum equations may be used to describe weak shock layers at low Mach numbers. The present contribution extends the steady laminar base flow model of Gilbarg and Paolucci [7] (GP) and the two-dimensional modal linear stability analysis Duck and Balakumar [6] by incorporating nonzero transverse and lateral shock velocity components. In line with earlier predictions, analysis of the GP base flow model did not reveal discrete eigenvalues or unstable members of the continuous spectrum. Three-dimensional perturbations were found to be stronger damped than their 2d counterparts, while less damped continuous branches are generated as the disturbance wavelength increases. Amplitude functions of the least damped perturbations exhibit a damped oscillatory nature toward the hot side of the shock. Non-modal linear stability and receptivity analyses are underway.

Keywords: shock layer, continuum, linear stability

Nomenclature

Latin

 M_1 – Mach number, $u_1/\sqrt{\gamma RT_1}$

 Re_1 – Unit Reynolds number, $\rho_1 u_1/\mu_1$ [1/m]

Re - Reynolds number, $\rho_1 u_1 \delta^* / \mu_1$

Greek

 λ_1 – Mean free path

Superscripts

q* - Dimensional flow quantity

 $\overline{\mathbf{q}}$ – Steady, laminar, base flow quantity

q – Amplitude function of modal perturbation Subscripts

1 - Indicates conditions at the shock cold side

1. Theory

1.1. Governing equations and non-dimensionalization

The non-dimensional compressible equations of motion written in tensor form in terms of density, ρ , velocity components, u_k , and temperature, T, read

$$\frac{\partial \rho}{\partial t} + \frac{\partial (\rho u_k)}{\partial x_k} = 0 \tag{1a}$$

$$\rho \left(\frac{\partial u_i}{\partial t} + u_k \frac{\partial u_i}{\partial x_k} \right) = -\frac{1}{\gamma M_1^2} \frac{\partial (\rho T)}{\partial x_i} + \frac{\partial \sigma_{ki}}{\partial x_k}$$
(1b)

$$\rho\left(\frac{\partial T}{\partial t} + u_k \frac{\partial T}{\partial x_k}\right) = -(\gamma - 1)\rho T \frac{\partial u_k}{\partial x_k} + \frac{\gamma}{RePr} \frac{\partial}{\partial x_k} \left(\frac{k}{k_1} \frac{\partial T}{\partial x_k}\right) + \frac{M_1^2 \gamma (\gamma - 1)}{Re} \Phi \tag{1c}$$

Here the ideal gas law has been used, body force terms have been neglected and the non-dimensional viscous stress tensor, σ_{ij} , and viscous dissipation function, Φ , are explicitly defined as

$$\sigma_{ij} = \frac{\mu}{Re} \left(\frac{\partial u_i}{\partial x_j} + \frac{\partial u_j}{\partial x_i} - \frac{2}{3} \delta_{ij} \frac{\partial u_k}{\partial x_k} \right) + \frac{\lambda}{Re} \delta_{ij} \frac{\partial u_k}{\partial x_k}, \tag{1d}$$

$$\Phi = \sigma_{ij} \frac{\partial u_i}{\partial x_j} = \mu \left(\frac{\partial u_i}{\partial x_j} + \frac{\partial u_j}{\partial x_i} - \frac{2}{3} \delta_{ij} \frac{\partial u_k}{\partial x_k} \right) \frac{\partial u_i}{\partial x_j} + \lambda \left(\frac{\partial u_k}{\partial x_k} \right)^2.$$
 (1e)

HiSST-2025-58 On Shock Layer Instabilities

¹Technion - Israel Institute of Technology, Haifa 32000, vassilis@technion.ac.il

alongside a non-dimensional equation of state

$$\gamma M_1^2 p = \rho T. \tag{1f}$$

The Prandtl number is taken to be a constant and evaluated at the cold side of the shock. It is used to express the coefficient of heat conductivity in terms of the first coefficient of viscosity, the latter taken to be a function of temperature alone.

Scales for density, velocities, pressure, temperature and viscosity are constructed using flow variables at the cold side of the shock,

$$\rho_1, u_1, \rho_1 u_1^2, T_1, \mu_1.$$
 (2a)

In addition to the above scales, a length scale, δ^* , to be discussed shortly, is used to construct a time scale,

$$\delta^*/u_1$$
. (2b)

1.2. On length scales in the shock layer

An ambiguity is introduced into the analysis by the absence of an obvious scale to non-dimensionalize lengths in the equations of motion, define a domain in which to solve (9) numerically, and consistently define the flow Reynolds number while maintaining the assumption of flow in the continuum regime. At a macroscopic level, Prandtl [13] and Becker [3] have defined a measure of the shock layer thickness, Δ^* ,

$$\Delta^* = \frac{u_1^* - u_2^*}{\max \left| \frac{du^*}{dx^*} \right|}.$$
 (3)

by reference to the velocity difference either side of the shock and the maximum value of the slope of the sigmoid curve describing the dependence of the streamwise velocity component.

On the other hand, at the microscopic level, the mean-free path [8, 5]

$$\lambda_1^* = \frac{16}{5} \sqrt{\frac{\gamma}{2\pi}} \frac{\mu_1}{\rho_1 a_1},\tag{4}$$

provides another length scale, calculated here with flow properties at the cold side of the shock, with a_1 the local speed of sound. In order to set the length scale and obtain physically meaningful results by the Navier-Stokes-Fourier equations that govern weak shocks in the continuum regime and the target altitudes, the present analysis is performed at a low constant value of the Knudsen number, $Kn=10^{-4}$. In addition, a low Mach number value is chosen, in order to preserve the relevance of results obtained by the Navier-Stokes-Fourier system. Indeed, the pioneering numerical works of Liepmann et al. [9, 10] and Bird [4] have established the non-Maxwellian (bimodal) internal shock structure postulated theoretically by Mott-Smith [12] at Mach numbers $M_1 \geq 2$, in contrast to the Maxwellian internal shock structure assumed by the continuum equations. The bimodal internal structure of strong shock layers has been verified in the celebrated experiments of Schmidt [15] and Alsmeyer [1, 2] and has since led to the acceptance of kinetic theory methods [4] as the appropriate tool to probe the internal structure of strong shocks. In the present work, the Mach number is taken to be $M_1 = 2$, to ensure that the continuum equations accurately describe the internal weak shock layer structure.

The Knudsen number, defined as the ratio of the mean free path, λ_1^* , and a characteristic flow length scale, δ^* ,

$$Kn = \frac{\lambda_1^*}{\delta^*},\tag{5}$$

is set in the present work at the constant value $Kn = 10^{-4}$, such that description of the internal shock layer structure by the continuum equations (1) be permissible. The relation between the flow Knudsen,

Mach and Reynolds numbers [14],

$$Kn = \sqrt{\frac{\gamma \pi}{2}} \frac{M_1}{Re},\tag{6}$$

is then used to determine the flow Reynolds number and, in turn, define the length scale δ^* on the basis of (5). Example conditions and flow parameters at which the present analysis is performed are shown in Table 1.

Table 1. International Standard Atmosphere (1976) atmospheric conditions, p_1, ρ_1, T_1 , at three altitudes and flow parameters calculated using $M_1 = 1.5, Kn = 10^{-4}$ and equations (3), (4), (5) and (6).

		Altitude [km]		
		20	30	40
p_1	[Pa]	5,475	1,172	278
$ ho_1$	$[imes 10^3~{ m kg}~{ m m}^{-3}]$	88	18	4
T_1	[K]	217	227	251
μ_1	$[imes 10^6 \; Pa \; s]$	14	15	16
Re_1	$[m^{-1}]$	2,784,571	543,600	119,000
a_1	$[m\;s^{-1}]$	295	302	318
u_1	$[m\;s^{-1}]$	443	453	476
λ_1	$[\times 10^7 \text{ m}]$	8.1	41.7	190.0
δ^*	[mm]	8.1	41.7	190.0

1.3. Linear Stability Analysis

1.3.1. The base flow

Linear modal instability analysis of a weak shock layer is performed by introducing the decomposition

$$\mathbf{q}(x, y, z, t) = \overline{\mathbf{q}}(x) + \varepsilon \widetilde{\mathbf{q}}(x, y, z, t); \quad \varepsilon \ll 1$$
(7)

into the governing equations (1). At ${\cal O}(1)$ the decomposition delivers the following steady laminar base flow equations

$$(\bar{\rho}\bar{u})' = 0 \tag{8a}$$

$$\bar{\rho}\bar{u}\bar{u}' = -\frac{1}{\gamma M_1^2} (\bar{\rho}\bar{T})' + \frac{1}{Re} \left[\left(2\bar{\mu}' + \bar{\lambda}' \right) \bar{u}' + \left(2\bar{\mu} + \bar{\lambda} \right) \bar{u}'' \right] \tag{8b}$$

$$\bar{\rho}\bar{u}\bar{v}' = \frac{1}{Re} \left[\bar{\mu}'\bar{v}' + \bar{\mu}\bar{v}'' \right] \tag{8c}$$

$$\bar{\rho}\bar{u}\bar{w}' = \frac{1}{Re}\left[\bar{\mu}'\bar{w}' + \bar{\mu}\bar{w}''\right] \tag{8d}$$

$$\bar{\rho}\bar{u}\bar{T}' = -(\gamma - 1)\bar{\rho}\bar{T}\bar{u}' + \frac{\gamma}{RePr}\left[\bar{k}'\bar{T}' + \bar{k}\bar{T}''\right] + \frac{M_1^2\gamma(\gamma - 1)}{Re}\left[(2\bar{\mu} + \bar{\lambda})(\bar{u}')^2 + \bar{\mu}(\bar{v}')^2 + \bar{\mu}(\bar{w}')^2\right] \tag{8e}$$

System (8) extends that originally derived (in dimensional form) and solved by Gilbarg and Paolucci [7], in that it accounts for (weak) oblique (planar) shock layers in which in-plane velocity components, $\bar{u}(x)$ and $\bar{v}(x)$, as well as an out-of-plane base flow component, $\bar{w}(x)$, exist.

In the absence of the velocity components \bar{v} and \bar{w} , using the equation of state to replace pressure by density and temperature and substituting the equation of continuity into those of momentum and

energy to eliminate density, the system of coupled nonlinear ordinary differential equations for \bar{u} and \bar{T} results,

$$\frac{2\bar{\mu} + \bar{\lambda}}{Re} \bar{u}_x = \bar{u} + \frac{1}{\gamma M_1^2} \frac{\bar{T}}{\bar{u}} - 1 - \frac{1}{\gamma M_1^2}, \tag{9a}$$

$$\frac{1}{(\gamma - 1)M_1^2RePr}\bar{T}_x = \frac{1}{\gamma(\gamma - 1)M_1^2}\bar{T} - \frac{1}{2}\bar{u}^2 + \left[1 + \frac{1}{\gamma M_1^2}\right]\bar{u} - \frac{1}{(\gamma - 1)M_1^2} - \frac{1}{2}.$$
 (9b)

Boundary conditions for this system are provided by the Rankine-Hugoniot conditions

$$u_1 = 1$$
 , $u_2 = \frac{\gamma - 1}{\gamma + 1} + \frac{2}{(\gamma + 1)M_1^2}$, (9c)

$$T_1 = 1$$
 , $T_2 = \frac{\left(\gamma M_1^2 - M_1^2 + 2\right)\left(1 - \gamma + 2\gamma M_1^2\right)}{(\gamma + 1)^2 M_1^2}$. (9d)

which are derived from (9a-9b) far upstream and downstream of the shock layer. The dimensional version of system (9) was first presented and solved in [7], while Duck and Balakumar [6] also used this shock layer model, although the Reynolds number does not appear explicitly in the latter analysis. Here the system is converted into one of first-order ordinary differential equations and solved numerically by straightforward shooting methods, once a viscosity-temperature law and appropriate boundary conditions have been specified. The Mach and Reynolds numbers are chosen to be consistent with weak shock layers and relevant to endoatmospheric flight at altitudes $20 \text{km} \leq h \leq 40 \text{km}$, as discussed in section § 1.2.

1.3.2. Modal linear stability analysis

Linearization of the state vector in primitive variables $\mathbf{q}=(\rho,u,v,w,T)^{\mathsf{T}}$ about the vector of steady basic flow components $\overline{\mathbf{q}}=(\bar{\rho},\bar{u},0,0,\bar{T})^{\mathsf{T}}$, obtained from solution of (9), neglecting terms of $O(\varepsilon^2)$ and solving the resulting system at $O(\varepsilon)$ for the determination of the perturbations $\widetilde{\mathbf{q}}$ results in an Initial Value Problem (IVP)

$$\mathcal{B}(\overline{\mathbf{q}}; Re; M_1) \frac{\partial \widetilde{\mathbf{q}}}{\partial t} = \mathcal{A}(\overline{\mathbf{q}}; Re; M_1) \widetilde{\mathbf{q}}$$
(10)

for the determination of the small-amplitude perturbations. Here, the modal Ansatz

$$\widetilde{\mathbf{q}}(x, y, z, t) = (\widetilde{\rho}, \widetilde{u}, \widetilde{v}, \widetilde{w}, \widetilde{\theta})^{\mathsf{T}} = \widehat{\mathbf{q}}(x) \exp\left[\mathrm{i}(\beta y + \delta z - \omega t)\right]; \quad \varepsilon \ll 1$$
(11)

is made to introduce harmonic in time perturbations and convert the IVP (10) into an eigenvalue problem (EVP)

$$\mathcal{A}\widehat{\mathbf{q}} = \omega \mathcal{B}\widehat{\mathbf{q}} \tag{12}$$

for the determination of the complex eigenvalue ω and the eigenvector $\hat{\mathbf{q}}=(\hat{\rho},\hat{u},\hat{v},\hat{w},\hat{\theta})^{\mathsf{T}}$, comprising of the complex amplitude functions of the linear perturbations in a temporal context, with $\mathbf{i}=\sqrt{-1}$ and $\beta=2\pi/L_y$ and $\delta=2\pi/L_z$ real wavenumber parameters along the y- and z- directions respectively. The (direct) linearized continuity, momentum and energy equations read

$$\begin{split} \left(\bar{u}\mathcal{D} + \mathcal{D}\bar{u}\right)\hat{\rho} + \left(\bar{\rho}\mathcal{D} + \mathcal{D}\bar{\rho}\right)\hat{u} + i\beta\bar{\rho}\hat{v} + i\delta\bar{\rho}\hat{w} \\ &= i\omega\hat{\rho} \end{split} \tag{13a}$$

$$\left(\hat{\rho}\bar{u}\mathcal{D}\bar{u} + \frac{1}{\gamma M_{1}^{2}}\mathcal{D}(\hat{\rho}\bar{T})\right)
+ \left[\bar{\rho}(\bar{u}\mathcal{D} + i\beta\bar{v} + i\delta\bar{w} + \mathcal{D}\bar{u}) - \frac{1}{Re}\left((\lambda + 2\mu)\mathcal{D}^{2} + (\lambda' + 2\mu')\mathcal{D}\bar{T} \cdot \mathcal{D} - \mu(\beta^{2} + \delta^{2})\right)\right]\hat{u}
+ \left[-\bar{\rho}\hat{u}\mathcal{D}\bar{u}_{y} - \frac{1}{Re}i\beta\left((\lambda + \mu)\mathcal{D} + \lambda'\mathcal{D}\bar{T}\right)\right]\hat{v}
+ \left[-\bar{\rho}\hat{u}\mathcal{D}\bar{u}_{z} - \frac{1}{Re}i\delta\left((\lambda + \mu)\mathcal{D} + \lambda'\mathcal{D}\bar{T}\right)\right]\hat{w}
+ \left[\frac{1}{\gamma M_{1}^{2}}\mathcal{D}(\bar{\rho})\right]\hat{T}
= i\omega\bar{\rho}\hat{u} \tag{13b}$$

$$\begin{split} \left(\hat{\rho}\bar{u}\mathcal{D}\bar{v} + \frac{i\beta\bar{T}}{\gamma M_{1}^{2}}\hat{\rho}\right) \\ &+ \left[\bar{\rho}\mathcal{D}\bar{v} - \frac{1}{Re}i\beta\left((\mu + \lambda)\mathcal{D} + \mu'\mathcal{D}\bar{T}\right)\right]\hat{u} \\ &+ \left[\bar{\rho}(\bar{u}\mathcal{D} + i\beta\bar{v} + i\delta\bar{w}) - \frac{1}{Re}\left(\mu\mathcal{D}^{2} + \mu'\mathcal{D}\bar{T}\cdot\mathcal{D} - \mu(\beta^{2} + \delta^{2}) - \lambda\beta^{2} - 2\mu\beta^{2}\right)\right]\hat{v} \\ &+ \left[\frac{\beta\delta\mu}{Re}\right]\hat{w} \\ &+ \left[\frac{i\beta\bar{\rho}}{\gamma M_{1}^{2}}\right]\hat{T} \\ &= i\omega\bar{\rho}\hat{v} \end{split} \tag{13c}$$

$$\left(\hat{\rho}\bar{u}\mathcal{D}\bar{w} + \frac{i\delta\bar{T}}{\gamma M_{1}^{2}}\hat{\rho}\right) \\
+ \left[\bar{\rho}\mathcal{D}\bar{w} - \frac{1}{Re}i\delta\left((\mu + \lambda)\mathcal{D} + \mu'\mathcal{D}\bar{T}\right)\right]\hat{u} \\
+ \left[\frac{\beta\delta\mu}{Re}\right]\hat{v} \\
+ \left[\bar{\rho}(\bar{u}\mathcal{D} + i\beta\bar{v} + i\delta\bar{w}) - \frac{1}{Re}\left(\mu\mathcal{D}^{2} + \mu'\mathcal{D}\bar{T}\cdot\mathcal{D} - \mu(\beta^{2} + \delta^{2}) - \lambda\delta^{2} - 2\mu\delta^{2}\right)\right]\hat{w} \\
+ \left[\frac{i\delta\bar{\rho}}{\gamma M_{1}^{2}}\right]\hat{T} \\
= i\omega\bar{\rho}\hat{w} \tag{13d}$$

$$\begin{split} &\left(\bar{u}\mathcal{D}\bar{T}+(\gamma-1)\bar{T}\mathcal{D}\bar{u}\right)\hat{\rho} \\ &+\left[\bar{\rho}\mathcal{D}\bar{T}+(\gamma-1)\bar{\rho}\bar{T}\mathcal{D}+\frac{\gamma(\gamma-1)M_{1}^{2}}{Re}\left((2\lambda+4\mu)(\mathcal{D}\bar{u})\mathcal{D}+2\mu(\mathcal{D}\bar{v})i\beta+2\mu(\mathcal{D}\bar{w})i\delta\right)\right]\hat{u} \\ &+\left[i\beta(\gamma-1)\bar{\rho}\bar{T}+i\beta\frac{2\gamma(\gamma-1)M_{1}^{2}\lambda}{Re}(\mathcal{D}\bar{u})+\frac{\gamma(\gamma-1)M_{1}^{2}}{Re}2\mu(\mathcal{D}\bar{v})\mathcal{D}\right]\hat{v} \\ &+\left[i\delta(\gamma-1)\bar{\rho}\bar{T}+i\delta\frac{2\gamma(\gamma-1)M_{1}^{2}\lambda}{Re}(\mathcal{D}\bar{u})+\frac{\gamma(\gamma-1)M_{1}^{2}}{Re}2\mu(\mathcal{D}\bar{w})\mathcal{D}\right]\hat{w} \\ &+\left[\bar{\rho}(\bar{u}\mathcal{D}+i\beta\bar{v}+i\delta\bar{w})+(\gamma-1)\bar{\rho}(\mathcal{D}\bar{u})-\frac{\gamma}{PrRe}\left(\mu\mathcal{D}^{2}+\mu'\mathcal{D}\bar{T}\cdot\mathcal{D}-\mu(\beta^{2}+\delta^{2})\right)\right]\hat{T} \\ &=i\omega\bar{\rho}\hat{T} \end{split} \tag{13e}$$

This system is discretized and the EVP (12) is converted into a generalized complex non-symmetric matrix eigenvalue problem

$$A\widehat{\mathbf{q}} = \omega B\widehat{\mathbf{q}},\tag{14}$$

with

$$A = \begin{pmatrix} A_{c\hat{\rho}} & A_{c\hat{u}} & A_{c\hat{v}} & A_{c\hat{w}} & A_{c\hat{\theta}} \\ A_{x\hat{\rho}} & A_{x\hat{u}} & A_{x\hat{v}} & A_{x\hat{w}} & A_{x\hat{\theta}} \\ A_{y\hat{\rho}} & A_{y\hat{u}} & A_{y\hat{v}} & A_{y\hat{w}} & A_{y\hat{\theta}} \\ A_{z\hat{\rho}} & A_{z\hat{u}} & A_{z\hat{v}} & A_{z\hat{w}} & A_{z\hat{\theta}} \\ A_{e\hat{\rho}} & A_{e\hat{u}} & A_{e\hat{v}} & A_{e\hat{w}} & A_{e\hat{\theta}} \end{pmatrix} \qquad B = \begin{pmatrix} 1 & 0 & 0 & 0 & 0 \\ 0 & \bar{\rho} & 0 & 0 & 0 \\ 0 & 0 & \bar{\rho} & 0 & 0 \\ 0 & 0 & 0 & \bar{\rho} & 0 \\ 0 & 0 & 0 & \bar{\rho} & 0 \end{pmatrix}$$

with the matrix entries inferred from (13). For receptivity studies, the adjoint eigenvalue problem $A^* \hat{\mathbf{q}}^* = -i\omega^* B^* \hat{\mathbf{q}}^*$ is defined, with the corresponding adjoint matrix entries presented in the Appendix.

2. Results

2.1. Base flow

The classic Gilbarg and Paolucci [7] case of $\bar{v}=\bar{w}=0$ is addressed here. Figure 1 presents results for the laminar steady streamwise basic flow velocity component, \bar{u} , and temperature, \bar{T} , and their streamwise derivatives at $M_1=1.5$ and two values of the Reynolds number, $Re=10^3$ and 10^4 , respectively. The absence of a length scale in this problem is evident in the results, where the order-of-magnitude increase in Re results exactly in one order-of-magnitude reduction of the shock layer thickness. The shock layer is indicated on the plots as a shaded region, the boundaries of which are defined by the base flow results having converged within 10^{-6} of their respective value predicted by the Rankine-Hugoniot conditions.

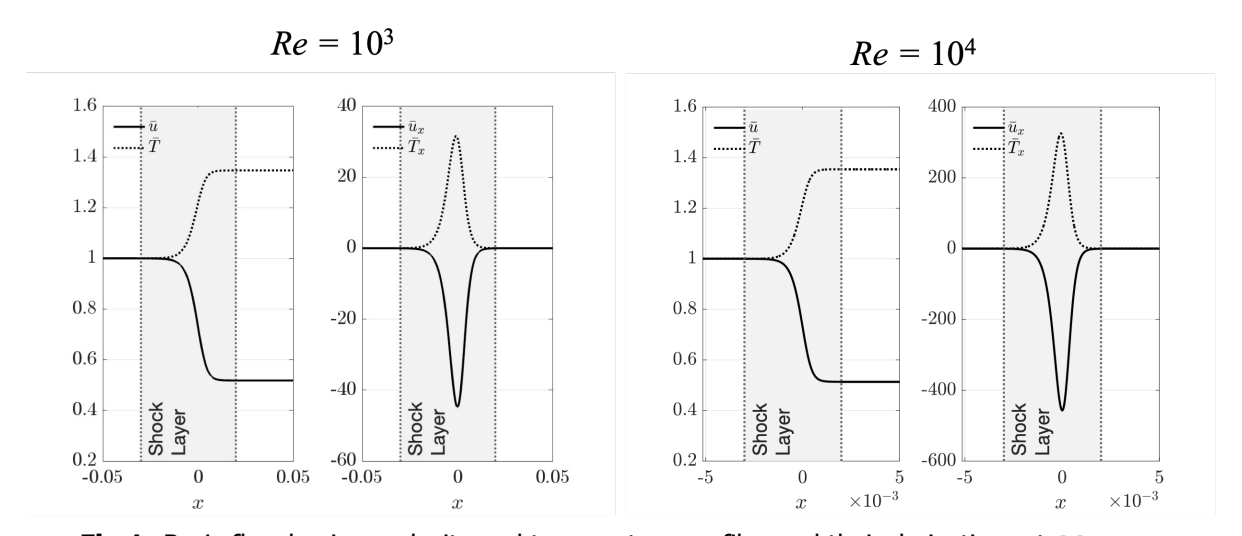


Fig 1. Basic flow laminar velocity and temperature profiles and their derivatives at $M_1=1.5$

2.2. The direct eigenspectrum

The present exploratory studies have used the QZ algorithm to perform full spectrum computations of (14) to identify and classify branches of eigenfunctions in the spectrum. The intricacy of the spectrum can be appreciated in Figure 2, where the imaginary part of the eigenvalue (damping rate), $\Im\{\omega\}$, is plotted against the real part (frequency), $\Re\{\omega\}$ using (from left to right) 256, 512, 1024 and 2048 spectral collocation points. Several observations are in order here. First, all eigenmodes are damped, $\Im\{\omega\} < 0$, indicating stability of the base flow solution at these conditions. Second, only continuous branches have been unraveled, a fact reflected in the relatively large number of discretization points required for convergence. Third, several lines of continuous spectrum have been found, qualitatively

identical with those discovered by Duck and Balakumar [6] in their related work. Of these, members of the near-horizontal least-damped branch will be discussed shortly.

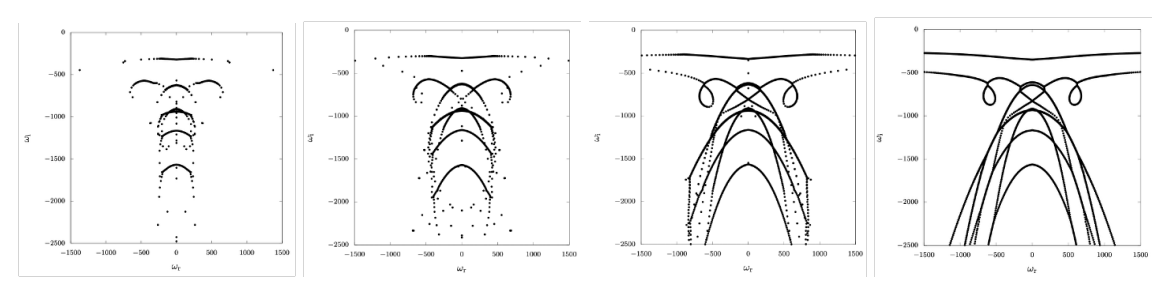


Fig 2. Convergence of the eigenspectrum at $M_1=1.5, Re=10^3$ and $\beta=2\pi/\lambda_1$

The next question addressed concerns stability of two- $(\beta \neq 0, \delta = 0)$ as opposed to three-dimensional $(\beta, \delta \neq 0)$ perturbations. Results shown in Figure 3 are representative of those obtained at a large number of Reynolds number, Mach number and wavenumber parameter combinations. On all occasions, the least-damped branch was barely affected, while stronger damped two-dimensional perturbation branches were found to be less damped than their three-dimensional counterparts.

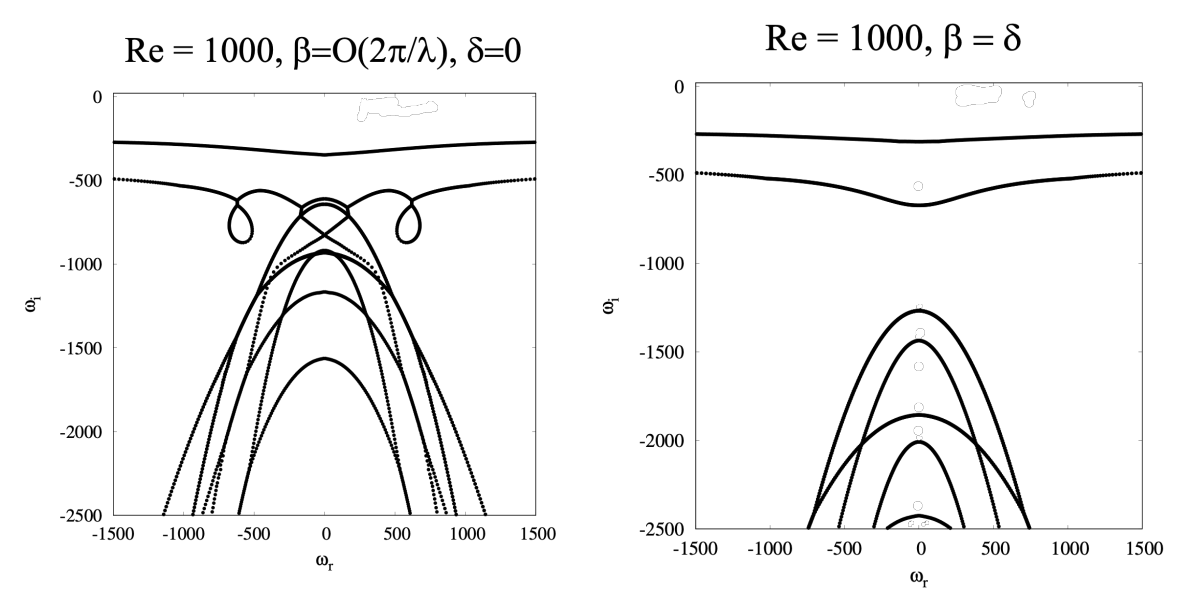


Fig 3. Representative result demonstrating modal stabilization of three-dimensional waves ($\delta \neq 0$) in relation to their two-dimensional counterparts ($\delta = 0$)

The parameter found to have the strongest effect on the shock layer eigenspectrum families is the wavenumber of perturbations, as shown in Figures 3 and 4. In Figure 4, results obtained for wavelengths of the order of the mean free path, $\lambda_1=2\pi/\beta_{\lambda_1}$, as well as those at twice and an order of magnitude larger are presented. Note that the same ordinate has been used in all three figures, indicating the tendency of the spectrum to become less stable for wavelengths increasingly larger than the mean free path and approaching pertinent to macroscopic length scales. However, no zero crossing has been found up to the largest wavelength examined.

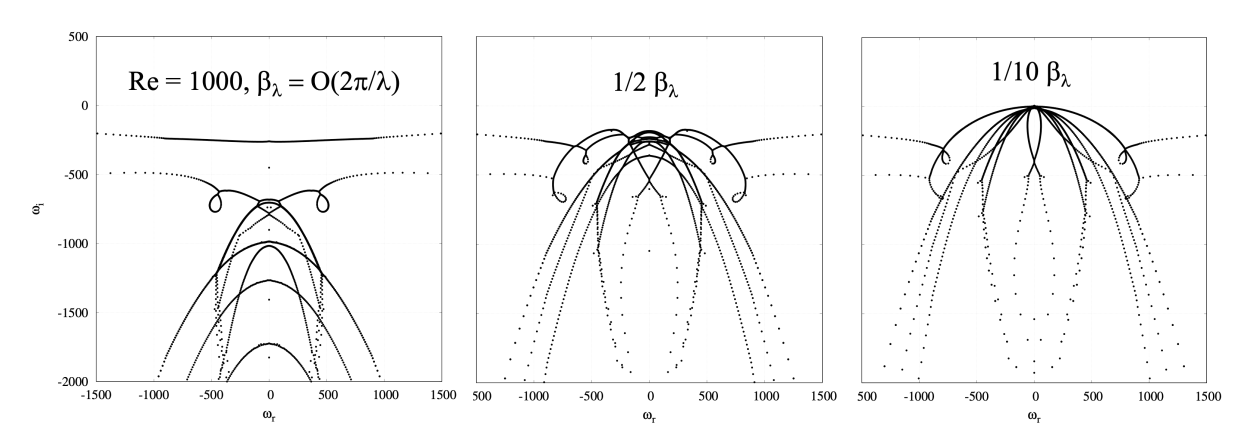


Fig 4. Destabilization of the eigenspectrum as the streamwise wavelength $\Lambda = 2\pi/\beta$ increases

Figure 5 presents amplitude functions of the transverse disturbance velocity component and disturbance temperature pertinent to a representative member of the least-damped branch of the continuous spectrum shown in figures 2 and 3. Results in the vicinity of the shock layer 1 are shown, since the amplitude functions reach the homogeneous Dirichlet boundary values imposed far away from the shock layer within a few mean-free path distances from the shock layer. The shape of the amplitude functions is qualitatively the same for all components of the eigenvector, namely monotonically increasing from $x\to -\infty$ and peaking near the center of the shock layer (defined as the location of the inflection point in the base flow velocity component), then turning into a damped exponentially decaying perturbation at x>0 and vanishing shortly after the disturbance has exited the shock layer.

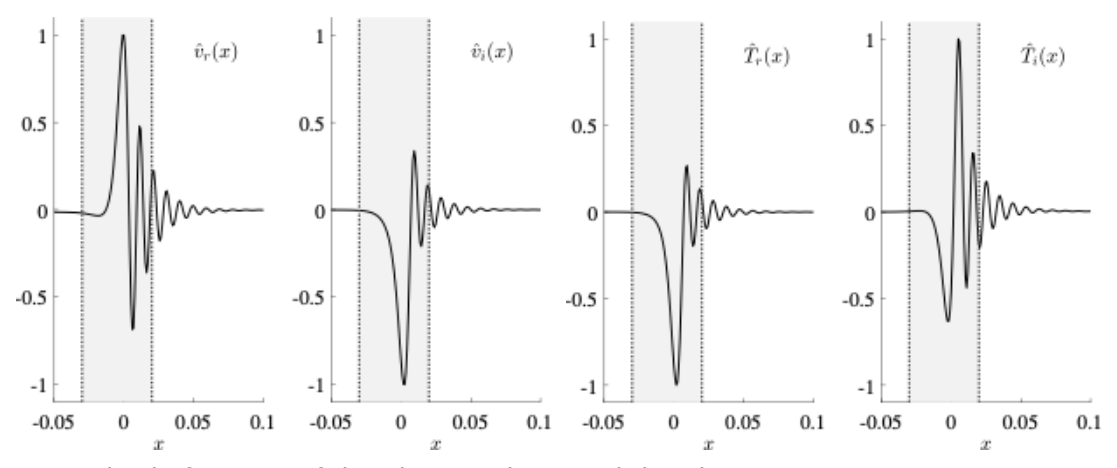


Fig 5. Amplitude functions of disturbance velocity and disturbance temperature at $M_1=1.5, Re=1000, \beta=\lambda_1$.

The absence of discrete modes and the damped nature of all eigenspectra computed at all parameters examined call for non-modal analysis, which is currently underway. In parallel, receptivity of the shock layer to incoming small-amplitude perturbations, extending the work of McKenzie and Westphal [11] into the viscous regime is also examined presently, and results will be reported elsewhere.

Acknowledgments

Research supported by ONR under Grant No. N000141202195 *Multi-scale modeling of unsteady shock-boundary layer hypersonic flow instabilities* with Dr. Eric Marineau as Program Officer

¹of the same extent as that shown in figure 1 at $Re = 10^3$

References

- [1] H. Alsmeyer. Nichtgleichgewichtsströmung von Gasen bei hohen Temperaturen, untersucht an Verdichtungsstössen in Argon und Stickstoff. *BMVg-FBWT Report 75-14*, 1975.
- [2] H. Alsmeyer. Density profiles in argon and nitrogen shock waves measured by the absorption of an electron beam. *Journal of Fluid Mechanics*, 74(3):497–513, 1976.
- [3] R. Becker. Stoßwelle und Detonation. Zeitschrift für Physik, 8:321–362, 1922.
- [4] G. A. Bird. Direct Simulation and the Boltzmann Equation. *Physics of Fluids*, 13(11):2676, 1970.
- [5] C. Cercignani. Rarefied gas dynamics: from basic concepts to actual calculations. CUP, 2000.
- [6] P. W. Duck and P. Balakumar. On the stability of normal shock waves. In M. Y. Hussaini et al., editor, *Instability, Transition and Turbulence*. Springer Verlag, NY, 1992.
- [7] D. Gilbarg and D. Paolucci. The structure of shock waves in the continuum theory of fluids. *J. Rat. Mech. and Anal.*, 2:617–642, 1953.
- [8] E. H. Kennard. Kinetic theory of gases. McGraw-Hill, 1938.
- [9] H. W. Liepmann, R. Narasimha, and M. T. Chahine. Structure of a plane shock layer. *The Physics of Fluids*, 5(11):1313–1324, 1962.
- [10] H. W. Liepmann, R. Narasimha, and M. T. Chahine. Theoretical and experimental aspects of the shock structure problem. In H. Görtler, editor, *Applied Mechanics - Proceedings of the Eleventh International Congress on Applied Mechanics*, pages 973–979. Springer-Verlag, Berlin, Heidelberg, 1966.
- [11] JF McKenzie and KO Westphal. Interaction of linear waves with oblique shock waves. *The Physics of Fluids*, 11(11):2350–2362, 1968.
- [12] H. M. Mott-Smith. The solution of the boltzmann equation for a shock wave. *Physical Review*, 82(6):885–892, 1951.
- [13] L. Prandtl. Gasbewegung. Handwörterbuch der Naturwissenschaften, 4:544–560, 1913.
- [14] S. A. Schaaf and P. L. Chambré. Flow of Rarefied Gases. Princeton University Press, 1961.
- [15] B. Schmidt. Electron beam density measurements in shock waves in Argon. *Journal of Fluid Mechanics*, 39(2):361–373, November 1969.

A. Entries of the adjoint matrix

Adjoint matrix (A_{ij}^*) entries

 $A_{11}^* = -\bar{u}\mathcal{D}$

$$\begin{array}{rcl} A_{13}^1 &=& -i \beta D \\ A_{13}^1 &=& -i \delta \rho \\ A_{15}^2 &=& 0 \\ \\ A_{15}^2 &=& 0 \\ \\ A_{21}^1 &=& u D u + \frac{1}{\gamma M_1^2} D T \\ A_{22}^1 &=& -D(\rho u) - i \beta \rho v - i \delta \rho w + \rho D u \\ && -\frac{1}{Re} \left[D^2 (\lambda + 2\mu) - D ((\lambda' + 2\mu') D \bar{T}) - \mu (\beta^2 + \delta^2) \right] \\ A_{23}^2 &=& \frac{i \beta}{Re} \left[-(\lambda + \mu) D - \mu' D \bar{T} \right] \\ A_{24}^2 &=& \frac{i \delta}{Re} \left[-(\lambda + \mu) D - \mu' D \bar{T} \right] \\ A_{25}^2 &=& \frac{1}{\gamma M_1^2} (-\bar{\rho} D) \\ A_{31}^2 &=& \bar{w} D \bar{v} - \frac{i \beta \bar{T}}{\gamma M_1^2} \\ A_{32}^2 &=& -\frac{i \beta}{Re} \left[-(\mu + \lambda) D - \lambda' D \bar{T} \right] \\ A_{33}^2 &=& -D(\rho \bar{u}) - i \beta \bar{\rho} \bar{v} - i \delta \bar{\rho} \bar{w} \\ && -\frac{1}{Re} \left[D^2 \mu - D(\mu' D \bar{T}) - \mu (\beta^2 + \delta^2) - \lambda \beta^2 - 2\mu \beta^2 \right] \\ A_{34}^2 &=& \frac{\beta \delta \mu}{Re} \\ A_{35}^2 &=& -\frac{i \beta \bar{\rho}}{\gamma M_1^2} \\ A_{41}^2 &=& \bar{w} D \bar{w} - \frac{i \delta \bar{U}}{\gamma M_1^2} \\ A_{42}^2 &=& \frac{i \delta}{Re} \left[-(\mu + \lambda) D - \lambda' D \bar{T} \right] \\ A_{43}^2 &=& \frac{\beta \delta \mu}{Re} \\ A_{44}^2 &=& -D(\rho \bar{u}) - i \beta \bar{\rho} \bar{v} - i \delta \bar{\rho} \bar{w} \\ && -\frac{1}{Re} \left[D^2 \mu - D(\mu' D \bar{T}) - \mu (\beta^2 + \delta^2) - \lambda \delta^2 - 2\mu \delta^2 \right] \\ A_{45}^2 &=& \frac{i \delta \rho}{\gamma M_1^2} \\ A_{45}^2 &=& \bar{\mu} D \bar{T} + (\gamma - 1) \bar{T} D \bar{u} \\ A_{51}^2 &=& \bar{\mu} D \bar{T} + (\gamma - 1) \bar{T} D \bar{u} \\ A_{52}^2 &=& \bar{\rho} D \bar{T} - D((\gamma - 1) \bar{\rho} \bar{T}) \\ && -\frac{i \delta \rho}{Re} \left[D((2\lambda + 4\mu) D \bar{w}) + 2\mu (D \bar{w}) i \beta + 2\mu (D \bar{w}) i \delta \right] \\ A_{53}^2 &=& -i \beta (\gamma - 1) \bar{\rho} \bar{T} - i \delta \frac{2\gamma (\gamma - 1) M_1^2}{Re} (D \bar{u}) - \frac{\gamma (\gamma - 1) M_1^2}{Re} D(2\mu D \bar{w}) \\ A_{54}^3 &=& -i \delta (\gamma - 1) \bar{\rho} \bar{T} - i \delta \frac{2\gamma (\gamma - 1) M_1^2}{Re} (D \bar{u}) - \frac{\gamma (\gamma - 1) M_1^2}{Re} D(2\mu D \bar{w}) \\ A_{54}^3 &=& -i \delta (\gamma - 1) \bar{\rho} \bar{T} - i \delta \frac{2\gamma (\gamma - 1) M_1^2}{Re} (D \bar{u}) - \frac{\gamma (\gamma - 1) M_1^2}{Re} D(2\mu D \bar{w}) \\ A_{54}^3 &=& -i \delta (\gamma - 1) \bar{\rho} \bar{T} - i \delta \frac{2\gamma (\gamma - 1) M_1^2}{Re} (D \bar{u}) - \frac{\gamma (\gamma - 1) M_1^2}{Re} D(2\mu D \bar{w}) \\ A_{54}^3 &=& -i \delta (\gamma - 1) \bar{\rho} \bar{T} - i \delta \frac{2\gamma (\gamma - 1) M_1^2}{Re} (D \bar{u}) - \frac{\gamma (\gamma - 1) M_1^2}{Re} D(2\mu D \bar{w}) \\ A_{54}^3 &=& -i \delta (\gamma - 1) \bar{\rho} \bar{T} - i \delta \frac{2\gamma (\gamma - 1) M_1^2}{Re} (D \bar{u}) - \frac{\gamma (\gamma - 1) M_1^2}{Re} D(2\mu D \bar{w}) \\ A_{54}^3 &=& -i \delta (\gamma - 1) \bar{\rho} \bar{T} - i \delta \frac{2\gamma (\gamma - 1) M_1^2}{Re} D(2\mu D \bar{u}) - \frac{\gamma (\gamma - 1) M_1^2}{Re} D(2\mu D \bar{u}) \\$$